Received: 25 July 2020 | Accepted: 6 December 2020

DOI: 10.1002/sctm.20-0346

TISSUE ENGINEERING AND REGENERATIVE MEDICINE

STEM CELLS TRANSLATIONAL MEDICINE

Cotransplantation of mesenchymal stem cells and endothelial progenitor cells for treating steroid-induced osteonecrosis of the femoral head

Haixia Xu[1] | Chengqiang Wang[1] | Chun Liu[1] | Ziyue Peng[1] | Jianjun Li[1] | Yanglei Jin[1] | Yihan Wang[1] | Jiasong Guo[1,2,3,4] | Lixin Zhu[1]

[1]Department of Spinal Surgery, Orthopedic Medical Center, Zhujiang Hospital, Southern Medical University, Guangzhou, People's Republic of China

[2]Department of Histology and Embryology, Southern Medical University, Guangzhou, People's Republic of China

[3]Key Laboratory of Tissue Construction and Detection of Guangdong Province, Guangzhou, People's Republic of China

[4]Institute of Bone Biology, Academy of Orthopaedics, Guangdong Province, Guangzhou, People's Republic of China

Correspondence

Jiasong Guo, PhD, Department of Histology and Embryology, Southern Medical University, Guangzhou 510515, People's Republic of China.
Email: jiasongguo@aliyun.com

Lixin Zhu, MD, Department of Spinal Surgery, Orthopedic Medical Center, Zhujiang Hospital, Southern Medical University, Guangzhou 510280, People's Republic of China.
Email: zhulixin1966@163.com

Funding information

Natural Science Foundation of Guangdong Province, Grant/Award Numbers: 2017A030312009, 2017A030313111; National Natural Science Foundation of China, Grant/Award Numbers: 81974329, 81672140

Abstract

Steroid-induced osteonecrosis of the femoral head (ONFH) is characterized by decreased osteogenesis, angiogenesis, and increased adipogenesis. While bone tissue engineering has been widely investigated to treat ONFH, its therapeutic effects remain unsatisfactory. Therefore, further studies are required to determine optimal osteogenesis, angiogenesis and adipogenesis in the necrotic area of the femoral head. In our study, we developed a carboxymethyl chitosan/alginate/bone marrow mesenchymal stem cell/endothelial progenitor cell (CMC/ALG/BMSC/EPC) composite implant, and evaluated its ability to repair steroid-induced ONFH. Our in vitro studies showed that BMSC and EPC coculture displayed enhanced osteogenic and angiogenic differentiation. When compared with single BMSC cultures, adipogenic differentiation in coculture systems was reduced. We also fabricated a three-dimensional (3D) CMC/ALG scaffold for loading cells, using a lyophilization approach, and confirmed its good cell compatibility characteristics, that is, high porosity, low cytotoxicity and favorable cell adhesion. 3D coculture of BMSCs and EPCs also promoted secretion of osteogenic and angiogenic factors. Then, we established an rabbit model of steroid-induced ONFH. The CMC/ALG/BMSC/EPC composite implant was transplanted into the bone tunnel of the rabbit femoral head after core decompression (CD) surgery. Twelve weeks later, radiographical and histological analyses revealed CMC/ALG/BMSC/EPC composite implants had facilitated the repair of steroid-induced ONFH, by promoting osteogenesis and angiogenesis, and reducing adipogenesis when compared with CD, CMC/ALG, CMC/ALG/BMSC and CMC/ALG/EPC groups. Thus, our data show that cotransplantation of BMSCs and EPCs in 3D scaffolds is beneficial in treating steroid-induced ONFH.

KEYWORDS

adipogenesis, angiogenesis, bone marrow mesenchymal stem cells, endothelial progenitor cells, osteogenesis, osteonecrosis of the femoral head

Haixia Xu, Chengqiang Wang, and Chun Liu contributed equally to this study.

1 | INTRODUCTION

Osteonecrosis of the femoral head (ONFH) is a serious disease that causes the femoral head to collapse, and is accompanied by secondary osteoarthritis.[1,2] Due to high morbidity and disability rates in young adults, ONFH has been a key research area in the orthopedic arena. Previous epidemiological studies have indicated that high-dose steroids are one of the main causes of ONFH.[3,4] While disease pathogenesis remains unclear, several mechanisms have been shown to contribute to the disease state, that is, elevated intramedullary pressure, imbalanced osteogenic and adipogenic differentiation of bone marrow mesenchymal stem cells (BMSCs), and impaired angiogenesis.[5,6]

Several hip-preserving surgical methods may be applied to treat early ONFH, that is, core decompression, bone graft and osteotomy[2,7,8]; however, these treatment modalities are ineffective, as >80% of patients with ONFH will ultimately require total hip arthroplasty (THA).[9] While THA procedures significantly improve patient quality of life, there is an increased risk of revision due to dislocation, periprosthetic fracture, infection, and prosthesis loosening after THA.[10,11] Therefore, THA cannot be considered the best therapeutic approach for ONFH, especially in relatively young patients.

Bone tissue engineering is a significant research area for treating ONFH; researchers have used specific cell groups to seed and promote bone regeneration, for example, BMSCs with their multidifferentiation capabilities.[12] However, inadequate osteogenic and angiogenic BMSC differentiation has restricted their application in treating ONFH. While several studies have enhanced BMSC osteogenic and angiogenic functions using gene transfection and the sustained release of growth factors from biomaterials,[13-16] methods for preventing potential hazards of gene-editing technologies and measures to achieve effective growth factor release must be investigated by further studies.[17,18] With their innate ability to repair damaged blood vessels, endothelial progenitor cells (EPCs) have also been used to treat ONFH; EPC injection into the femoral head promoted early vascularization and bone regeneration in steroid-induced ONFH, thereby promoting EPCs as a valid seeding source in treating ONFH.[19] However, EPCs cannot directly participate in bone regeneration, as they cannot differentiate into osteoblasts.

In recent years, several studies have revealed that a mixture of BMSCs and EPCs is advantageous over single cell types in repairing bone defects. BMSC/EPC coculture and cotransplantation systems have generated enhanced biological effects; for example, the in vitro coculture of BMSCs with EPCs significantly promoted osteogenic and angiogenic differentiation,[20] EPCs enhanced BMSC proliferation in three-dimensional (3D) coculture models,[21] and BMSCs reduced EPC apoptosis via direct cell-cell contacts.[22] Additionally, several in vivo studies have also shown that BMSC and EPC cotransplantation effectively facilitated osteogenesis and angiogenesis in bone defect models.[23,24] Nevertheless, the effects of cocultured cells on osteonecrosis therapy have been rarely studied. Some studies have observed that transplantation of bone marrow mononuclear cells (BMNCs) benefited bone repair in early ONFH[25-27]; however, BMNCs are a heterogeneous group of cells, consisting of larger proportions of lymphocytes, monocytes, and smaller proportions of hematopoietic stem cells, BMSCs and EPCs.[28] Whether bone repair effects primarily resulted from BMSCs and EPCs was not confirmed. In this study, we collected and expanded BMSCs and EPCs separately from BMNCs, to investigate if the combinatorial transplantation of BMSCs and EPCs was effective in treating steroid-induced ONFH. While we were cognizant that increased adipogenic differentiation could accelerate ONFH progression,[29] we asked whether a BMSC/EPC combination strategy could reduce adipogenesis in the femoral head.

Composite scaffolds can not only load and deliver seeding cells, but also provide 3D environments for cell growth and intercellular communications. Carboxymethyl chitosan (CMC) is a chitosan derivative, with improved biological and physicochemical properties, including biodegradability, biocompatibility, and water solubility at neutral pH.[30] Alginate (ALG) is a common natural polymer used in various fields such as the food and pharmaceutical industries.[31] CMC/ALG scaffolds are easy to fabricate, with an excellent biocompatibility in promoting bone formation.[32] In this study, we developed a CMC/ALG/BMSC/EPC composite implant, and applied it to the treatment of steroid-induced ONFH. We assessed the treatment effects of these CMC/ALG/BMSC/EPC composite implants on steroid-induced ONFH by examining osteogenesis, angiogenesis, and adipogenesis functionalities in the femoral head.

Significance statement

Cell-based therapy for skeletal diseases is limited by insufficient osteogenesis and angiogenesis. Cotransplantation of bone marrow derived mesenchymal stem cells (BMSCs) and endothelial progenitor cells (EPCs) can obviously promote bone regeneration and blood vessel formation in bone defect models. However, whether cotransplantation of BMSCs and EPCs can benefit the osteonecrosis repair is poorly investigated. Using a rabbit model, the present study evaluated the treatment effect of BMSCs/EPCs transplantation on steroid-induced osteonecrosis of the femoral head (ONFH). When seeded in carboxymethyl chitosan/alginate (CMC/ALG) scaffolds and then transplanted into the necrotic area of the femoral head, BMSCs/EPCs significantly promoted the repair of steroid-induced ONFH. The treatment effect was induced by enhanced osteogenesis and angiogenesis and reduced adipogenesis.

2 | MATERIALS AND METHODS

2.1 | Isolation and culture of BMSCs and EPCs

BMSCs and EPCs were isolated from 1 month-old New Zealand white rabbits, according to previously described methods.[33] Briefly, bone

marrow was aspirated into heparinized syringes from the tibia medullary cavity, followed by 1:1 dilution in phosphate-buffered saline (PBS; HyClone, USA). After carefully overlaying the diluted bone marrow onto an equal volume of Ficoll-Isopaque Plus (Solarbio, China), we performed density gradient centrifugation at 2000 rpm for 30 minutes to harvest BMNCs.

To generate BMSCs, BMNCs were resuspended in Dulbecco's modified Eagle's medium (DMEM; Gibco, USA), supplemented with 10% fetal bovine serum (FBS; Gibco), and 1% penicillin/streptomycin (HyClone). Cells were then seeded into 25 cm^2 culture flasks at 37°C, in a humidified atmosphere containing 5% CO_2. After 3 days, nonadherent cells were removed by changing the culture medium. To generate EPCs, BMNCs were resuspended in endothelial growth medium-2 (EGM-2; Lonza, USA) containing 10% FBS, 1% penicillin/streptomycin, and a growth factor bullet kit (Lonza). Cells were seeded into 25 cm^2 culture flasks precoated with rat tail collagen type I (BD, USA). After a 24 hours incubation at 37°C in 5% CO_2, nonadherent cells were removed by changing the culture medium. After this, BMSC and EPC culture medium was changed every 3 days. When the cells were at 80% to 90% confluence, they were trypsinized in 0.25% trypsin (Gibco) and passaged at a density of $1 \times 10^4/cm^2$. BMSCs and EPCs at passages 3 to 4 were used for subsequent assays.

2.2 | Multilineage differentiation potential of BMSCs

To assess the multilineage differentiation potential of BMSCs, we investigated osteogenic and adipogenic differentiation abilities.

For osteogenesis, BMSCs were cultured in osteogenic induction medium containing DMEM supplemented with 10% FBS, 1% penicillin/streptomycin, 10 nM dexamethasone (Sigma, USA), 50 mg/mL ascorbic acid (Sigma), and 10 mM β-glycerophosphate (Sigma). After 7 days, we performed alkaline phosphatase (ALP) staining. After 14 days, alizarin red S staining was also performed to identify calcium deposits.

For adipogenesis, cells were cultured in adipogenic induction medium containing DMEM supplemented with 10% FBS, 1% penicillin/streptomycin, 0.5 mM 1-methyl-3-isobutylxanthine (Sigma), 1 mM dexamethasone, 10 mg/mL insulin (Sigma), and 100 mM indomethacin (Sigma). After 14 days, oil red O solution was used to visualize cytoplasmic lipid vacuoles. These studies were independently performed three times.

2.3 | Functional identification of EPCs

We evaluated EPC function by assessing their ability to take up 1,1′-dioctadecyl-3,3,3′,3′-tetramethylindocarbocyanine perchlorate-labeled acetylated low-density lipoprotein (DiI-Ac-LDL; Molecular Probes, USA), and bind fluorescein isothiocyanate-labeled *Ulex europaeus* agglutinin-1 (FITC-UEA-1; Sigma). Briefly, EPCs were incubated with 10 μg/mL DiI-Ac-LDL for 4 hours. After washing three times in PBS, cells were fixed in 4% paraformaldehyde (PFA; Leagene, China) for 15 minutes. Then, cells were stained with 50 μg/mL FITC-UEA-1 for 1 hour. Images were acquired using a fluorescence microscope (Zeiss, Germany). These experiments were independently performed three times.

2.4 | Flow cytometric analysis

BMSCs and EPCs were trypsinized to generate 1×10^6 cells. To confirm BMSC phenotypes, cells were incubated with monoclonal mouse antibodies against CD29 (5 μg/mL, Sigma), CD90 (5 μg/mL, Abcam, UK), CD45 (5 μg/mL, Genetex, USA), and CD34 (2 μg/mL, Genetex). Antibodies against CD31 (5 μg/mL, Genetex) and kinase insert domain-containing receptor (KDR, 5 μg/mL, Abcam) were used to verify EPC phenotypes. After primary antibody incubation, cells were washed three times in PBS, and then incubated with rat anti-mouse IgG secondary antibodies (4 μg/mL, BD) labeled with fluorescent markers including FITC, phycoerythrin (PE), and BD Horizon V450. Cell fluorescence was detected using a four-color multiparameter flow cytometer (FACSVerse, BD). All experiments were independently performed three times.

2.5 | Coculture of BMSCs and EPCs

In coculture systems, BMSCs and EPCs were seeded into 24-well culture plates (8×10^4 cells/well) at ratios of 1:0, 1:1, and 0:1 respectively, and cultured for 7 days in different culture media. To investigate osteogenesis, cells were cultured in a 1:1 mixture of osteogenic media and EGM-2. Assays evaluating osteogenesis included ALP staining, ALP activity and real-time polymerase chain reaction (RT-PCR).

To evaluate adipogenesis, cells were cultured in a 1:1 mix of adipogenic media and EGM-2. Oil red O staining, quantification of lipid accumulation and RT-PCR were conducted to evaluate adipogenesis.

To investigate angiogenesis, cells were cultured in EGM-2, after which their angiogenic capacity was assessed by tube formation assay and RT-PCR.

2.6 | ALP staining and activity assays

ALP staining was performed according to the protocol from the 5-bromo-4-chloro-3-indolyl phosphate/nitro blue tetrazolium chloride (BCIP/NBT) ALP Color Development Kit (Beyotime). Images were generated using light microscopy (Leica, Germany). ALP activity was evaluated using the ALP Activity Detection Kit (Beyotime) following manufacturer's instructions. Cells were washed twice in PBS and then lysed on ice in 0.1% Triton X-100 (Sigma). After centrifugation at 12000 rpm for 15 minutes at 4°C, supernatants were collected. ALP activity was examined by colorimetric assay using p-nitrophenyl

phosphate as the ALP substrate. Quantification of the formed p-nitrophenol was measured at 405 nm on a spectrophotometer (ELX808, BioTek, USA). The bicinchoninic acid (BCA) protein assay kit (Beyotime) was used to determine protein concentrations. ALP activities were normalized to protein concentrations. All experiments were independently performed three times.

2.7 | Oil red O staining and lipid accumulation assay

Oil red O staining was performed according to instructions from the Oil red O Staining Kit (Yuanye Bio-Technology, China). Briefly, cells were fixed in 4% PFA and stained in freshly prepared Oil red O solution for 20 minutes. After washing three times in water, cells were visualized with a microscope (Leica), and images recorded. For the lipid accumulation assay, Oil red O was dissolved in isopropanol (Aladdin, China), and the absorbance at 510 nm recorded as previously described. All experiments were independently performed three times.

2.8 | In vitro tube formation assay

Cells were seeded onto culture plates coated with Matrigel (BD, USA) at a density of 8×10^4 cells/well. They were then incubated at 37°C in 5% CO_2 for 6 to 8 hours. Capillary-like structures were observed under an inverted phase contrast microscope (Leica, Germany). All experiments were independently performed three times.

2.9 | Quantitative RT-PCR

Total RNA was extracted using TRIzol reagent (Invitrogen, USA). Then, reverse transcription reactions were conducted using an M-MLV Reverse Transcription Kit (Takara, Japan). We analyzed the expression of runt-related transcription factor 2 (Runx2), bone morphogenetic protein 2 (BMP-2), peroxisome proliferator-activated receptor-gamma (PPAR-γ), CCAAT/enhancer binding protein alpha (C/EBPα), KDR, and matrix metalloproteinase 3 (MMP-3) using a SYBR Green PCR Mix (Takara). The housekeeping gene, glyceraldehyde-3-phosphate dehydrogenase (GAPDH) was used to normalize mRNA levels. The RT-PCR cycling conditions were; 95°C for 30 seconds, and 40 cycles at 95°C for 5 seconds and 60°C for 30 seconds. Specific primer sequences are listed (Table 1). All experiments were independently performed three times.

2.10 | Preparation of CMC/ALG scaffolds

CMC/ALG scaffolds were prepared by physical cross-linking and freeze-drying techniques as previously described.[32] Briefly, 750 mg CMC (Macklin, China) and 750 mg ALG (Sigma) were added to 50 mL deionized water. The mixture was stirred until all the powder was dissolved. The solution was poured into molds with an inner diameter of 3 mm, and frozen overnight at −80°C. The frozen mixture was then lyophilized in a lyophilizer (Alpha1-2, Christ, Germany) for 24 hours. After this, scaffolds were cross-linked with 2% $CaCl_2$ solution and freeze-dried again. Epoxyethane was then used to sterilize the CMC/ALG scaffolds.

2.11 | Scanning electron microscopy

Scaffold surface morphology and microstructures were examined by scanning electron microscopy (SEM; Hitachi S-3000N, Japan). Samples were coated with a thin layer of gold prior to SEM observations. Then, pore sizes of the CMC/ALG scaffolds were determined.

2.12 | CMC/ALG scaffold cytotoxicity

We considered the effects of scaffold extract liquid on cell viability as indicative of scaffold cytotoxicity. The Cell Counting Kit-8 (CCK-8; Dojindo Laboratories, Japan) assay was used to evaluate the cytotoxicity of EGM-2 preconditioned cells in the presence of CMC/ALG scaffolds. BMSC and EPC cocultures were established in 96-well plates at a density of 1×10^3 cells/well, and were cultured with EGM-2 or scaffold extract liquid. Cell viability was assessed at day 1, 3, 5, and 7 by adding 10 μL CCK-8 solution to each well. After 1 hour incubation at 37°C, the optical density was measured at 450 nm. All experiments were independently performed three times.

2.13 | Cell adhesion to CMC/ALG scaffolds

To investigate cell adhesion to CMC/ALG scaffolds, BMSCs were labeled with DiI (Beyotime), and EPCs were labeled with 3,3′-dioctadecyloxacarbocyanine perchlorate (DiO; Beyotime). After scaffolds were sliced into thin layers, a 1:1 mix of BMSCs and EPCs was seeded with scaffolds, and incubated for 3 days. Cell adherence to scaffolds was assessed and observed using a confocal laser scanning microscope (Leica). All experiments were independently performed three times.

2.14 | Angiogenic differentiation and live/dead staining of cocultured cells on CMC/ALG scaffolds

CMC/ALG scaffold samples were coated with Matrigel and placed into confocal dishes. Approximately 100 μL cell suspensions (1×10^6 cells/mL) consisting of equal quantities of BMSCs and EPCs were seeded into scaffold samples, and cultured for 3 days. After this period, scaffolds were stained with calcein AM (KeyGEN, China) and propidium iodide (PI; KeyGEN) for 30 minutes. Cells on scaffolds were

TABLE 1 Primer sequences for real-time polymerase chain reaction

Gene	Forward primer sequence	Reverse primer sequence
Runx2	AGAGTAGGTGTCCCGCCTCA	GAGGAACAGGGTGGTGGAAGAC
BMP-2	ACAAGTGGGAAAACCACCCG	GATGGAAACCGCTGTCGTCT
PPAR-γ	GACGACAGACAAATCACCGTTT	ATGCGGATGGCGACTTCTTT
C/EBPα	CGGGAACGCAACAACATCG	AGGCGGTCATTGTCACTGGT
KDR	AGCAGGGTGGCAAAGACTAC	CGACTGGTTGTCATCTGGGA
MMP-3	GGACAAAGGATACAACAGGAACC	AGGGACAGGTTCCATAGGCA
GAPDH	TCGGAGTGAACGGATTTGGC	CCAGCATCACCCCACTTGAT

observed using confocal laser scanning microscopy (Leica). All experiments were independently performed three times.

2.15 | Enzyme-linked immunosorbent assay

In total, 1×10^6 BMSCs and EPCs were seeded in scaffolds in ratios of 1:0, 1:1, and 0:1. After 7 days of culture, the culture medium was collected to quantify ALP, BMP-2, insulin-like growth factor 1 (IGF-1), MMP-3, platelet-derived growth factor (PDGF), and vascular endothelial growth factor (VEGF) levels using enzyme-linked immunosorbent assay kits from MEIMIAN, China. Three independent experiments were performed.

2.16 | Induction of an early ONFH rabbit model

All animal experiments were performed in accordance with Institutional Animal Care and Use committee guidelines and approved protocols at the Southern Medical University. Sixty male New Zealand white rabbits, with an average weight of 3 kg were used. The early ONFH model was induced by a combination of lipopolysaccharide (LPS; Sigma) and methylprednisolone (MPS; Pfizer, USA), as previously described.[34] All rabbits were intravenously injected with LPS (10 μg/kg). After 24 hours, MPS at 20 mg/kg body weight was injected intramuscularly three times, at 24 hours intervals. When the MPS was injected, 100 000 U of penicillin was also injected intramuscularly to prevent infection. During model set-up, five rabbits died of infection. After 6 weeks, the 55 remaining rabbits were examined by magnetic resonance imaging (MRI) to establish if ONFH was present. Ultimately, 42 rabbit models of ONFH were successfully established. Of these, two rabbits were sacrificed for microcomputed tomography (CT) (ZKKS-MCT-Sharp, China) and hematoxylin and eosin (H&E) staining of the femoral head. The others underwent surgical treatment.

2.17 | Groupings and surgical procedures

Forty rabbits with early ONFH were divided into five groups: (a) the core decompression (CD) group; (b) the CMC/ALG group; (c) the CMC/ALG/BMSC (1×10^7 cells) group; (d) the CMC/ALG/EPC (1×10^7 cells) group, and (e) the CMC/ALG/BMSC/EPC (5×10^6 BMSCs and 5×10^6 EPCs) group. Rabbits were anesthetized by intravenous injection of 3% pentobarbital sodium (1 mL/kg). A 30 mm skin incision on the right hip was created, and the greater trochanter of the femur was exposed. Then, core decompression was performed by creating a bone tunnel from the greater trochanter to the femoral head, using a 3 mm diameter drill bit under the C-arm of an X-ray machine. The bone tunnel length was approximately 27 mm. Different implants were transplanted into the femoral head through this bone tunnel. Finally, the incision was sutured layer by layer.

2.18 | Radiological analysis

At 12 weeks postsurgery, rabbits were sacrificed by air embolism. Then, the right femoral head was harvested for micro-CT scanning. The instrument was set at 70 kV and 100 μA, with a voxel resolution of 10 μm. 3D images were reconstructed in the region of interest (ROI) of the femoral head. Trabecular bone parameters, including bone mineral density (BMD) and bone volume/total volume (BV/TV) were collected by associated software (ZKKS-MicroCT4.1). The radiology region for analysis is shown in Figure S1.

2.19 | Histopathology and immunohistochemistry

After radiological analysis, samples were fixed in 4% PFA for 48 hours, then decalcified in 10% ethylenediamine tetraacetic acid (EDTA; Leagene) for 6 weeks. To perform H&E and immunohistochemistry staining, samples were embedded in paraffin and cut into 5 μm sections. H&E staining was used to detect empty lacuna under light microscopy (Leica). Immunohistochemistry staining was also performed to examine osteogenic, adipogenic and angiogenic differentiation using, osteocalcin (OCN; GeneTex), adiponectin (GeneTex) and CD31 (GeneTex), respectively. Briefly, sections were fixed and stained with primary antibodies, followed by incubation with secondary antibodies (Abcam) conjugated to horse radish peroxidase (HRP). Peroxidase activity was visualized with diaminobenzidine (Sigma). Immunohistochemical images were observed using light microscopy (Leica). The histology and immunohistochemistry region for analysis is shown in Figure S1.

2.20 | Statistical analysis

All data were expressed as the mean ± SE of the mean (SEM). Statistical analysis was performed using SPSS 24.0 software. Student's *t*-test was used to examine differences between two groups. When multiple groups were compared, a one-way analysis of variance (ANOVA) was used. *P* values <.05 were considered statistically significant.

3 | RESULTS

3.1 | Characterization of BMSCs and EPCs

Both BMSCs and EPCs were characterized by morphology, function, and surface markers. Cultured BMSCs exhibited a fibroblast-like and long spindle-shaped morphology (Figure 1A). Their osteogenic differentiation potential was confirmed by positive ALP (Figure 1B) and alizarin red S (Figure 1C) staining. Their adipogenic differentiation potential was verified by positive Oil red O staining (Figure 1D). BMSCs expressed the typical MSC markers, CD29, and CD90, but were negative for the hematopoietic markers, CD45, and CD34 (Figure 1E).

Isolated EPCs displayed a round or spindle-shaped morphology on day 5 (Figure 1F) and day 10 (Figure 1G). After 2 weeks of culture, they exhibited a cobblestone-like morphology (Figure 1H). When seeded and incubated on Matrigel for 6 to 8 hours, EPCs formed capillary-like structures (Figure 1I). These cells also took up DiI-Ac-LDL and bound FITC-UEA-1 (Figure 1J). Flow cytometric analysis indicated that cells highly expressed both CD31 and KDR markers (Figure 1K).

3.2 | BMSC and EPC coculture enhance osteogenic and angiogenic differentiation, while adipogenic differentiation is decreased

The BMSC/EPC group exhibited the highest ALP expression and activity, followed by the BMSC group, whereas the EPC group barely expressed ALP (Figure 2A,B). The Oil red O staining and lipid accumulation assays revealed that the BMSC/EPC group had fewer lipid vacuoles when compared with the BMSC group, but the least number of lipid vacuoles were detected in the EPC group (Figure 2C,D). In addition, the tube formation assay demonstrated that tube numbers were highest in the BMSC/EPC group, followed by the EPC group and then the BMSC group (Figure 2E,F).

RT-PCR results (Figure 2G) revealed that expression of the osteogenesis-associated markers, Runx2 and BMP-2, and the angiogenesis-associated markers, KDR and MMP-3 were higher in the BMSC/EPC group than other groups. Also, expression of the adipogenic-associated markers, PPAR-γ, C/EBPα in BMSC/EPC and EPC groups were lower than the MSC group.

3.3 | CMC/ALG scaffolds show good biocompatibility, and 3D coculture of BMSCs and EPCs enhance osteogenic and angiogenic factor secretion

Cylindrical CMC/ALG scaffolds were approximately 3 mm in diameter and 27 mm long (Figure 3A). Porous interconnected structures were also observed by SEM (Figure 3B). CCK-8 assay results confirmed that CMC/ALG scaffolds generated no cytotoxicity effects on BMSC/EPC viability (Figure 3C). After seeding DiI labeled BMSCs and DiO labeled EPCs onto scaffolds, both cell types easily adhered to scaffolds (Figure 3D). The 3D distribution of cocultured cells on scaffolds was observed by laser scanning confocal microscopy (Figure 3E). Live/dead staining and tube formation assay data from 3D scaffolds demonstrated few dead cells, whereas most living cells formed tubular structures (Figure 3F). The 3D tubular structures formed by BMSCs/EPCs were observed by confocal microscopy (Figure 3G). After 7 days incubation on CMC/ALG scaffolds, cocultured cells released higher concentrations of the osteogenic factors, ALP, BMP-2, and IGF-1, and the angiogenic factors, MMP-3, PDGF, VEGF, when compared with both BMSCs and EPCs (Figure 3H).

3.4 | Establishment of a steroid-induced ONFH model and surgical procedures

The steroid-induced ONFH model was confirmed by MRI, micro-CT and H&E staining. The femoral head signal of the control group was normal in both T1-weighted MRI images (T1WI) and T2-weighted MRI images (T2WI) (Figure 4A). However, rabbits with steroid-induced ONFH showed a low signal in T1WI, and a high signal in T2WI (Figure 4B). When compared with the normal femoral head (Figure 4C), the necrotic femoral head showed thinner bone trabecula (Figure 4D). H&E staining showed that the normal femoral head was filled with eosin-stained nuclei (Figure 4E), while plenty of empty lacuna were observed in the model group (Figure 4F).

As shown, the surgical procedure involved core decompression (Figure 4G) and implantation (Figure 4H). Figure 4I depicts the greater trochanter of the femur under the incision, while Figure 4J shows the opening of the decompression channel. Figure 4K shows the implantation process and Figure 4L shows incision suturing.

3.5 | CMC/ALG/BMSC/EPC transplantation enhances bone reparation in vivo

Radiological evaluation of bone reparation was performed by micro-CT. The results showed that the CD group was severely disordered with loss of bone trabecula (Figure 5A). The CMC/ALG group showed some improvement in bone reparation (Figure 5A). Neither the CMC/ALG/BMSC group nor the CMC/ALG/EPC group promoted significant bone regeneration, however, the reparation effects in the CMC/ALG/BMSC/EPC group were marked (Figure 5A). As indicated

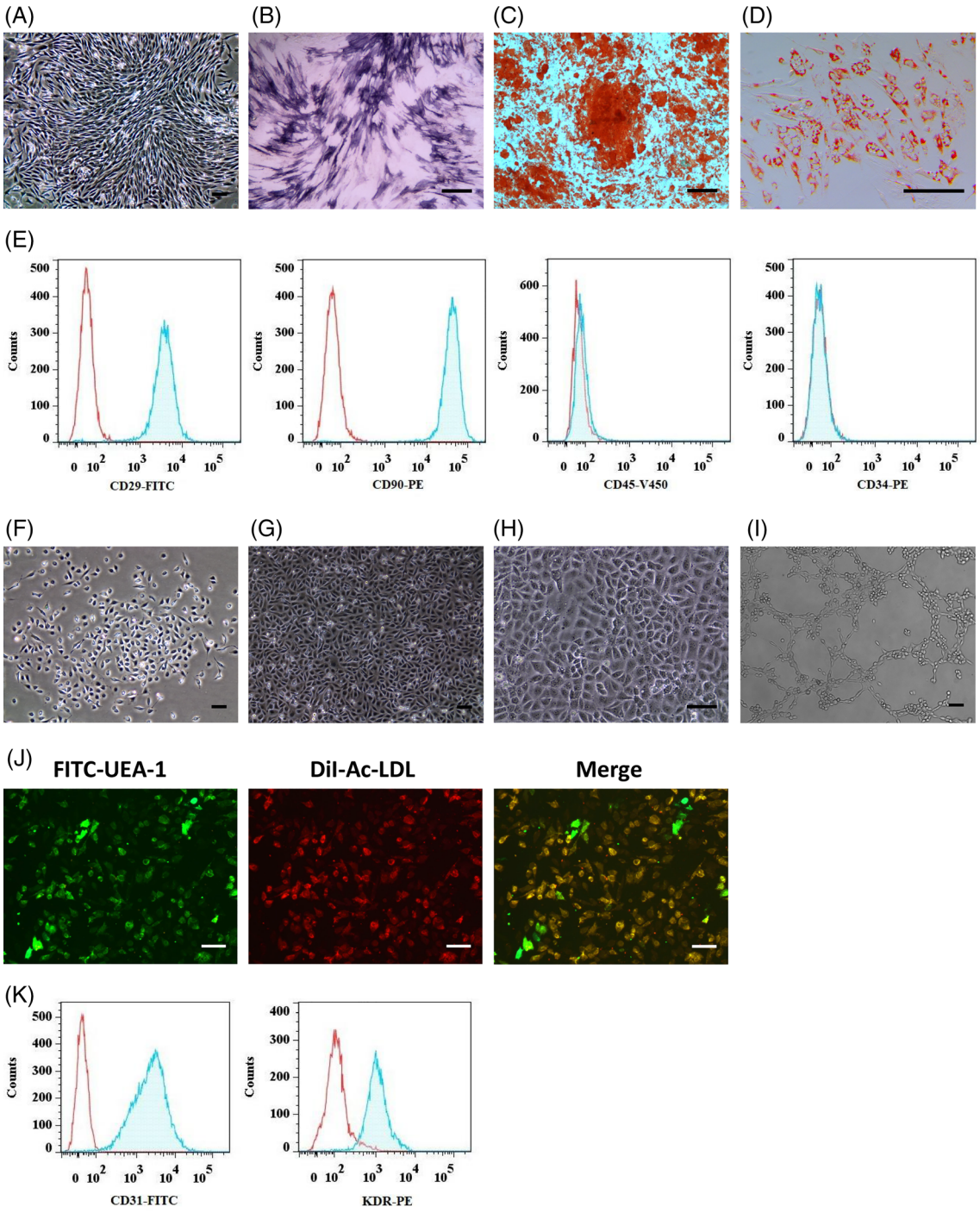

FIGURE 1 Characterization of BMSCs and EPCs. A, Isolated BMSCs showed a fibroblast-like and long spindle-shaped morphology. B, Osteogenic differentiation of BMSCs was assessed by ALP staining. C, Mineralized nodules were detected by Alizarin red S staining. D, Adipogenic differentiation of BMSCs was assessed by Oil red O staining. E, Flow cytometry analysis of the expression of BMSC surface markers. F, Isolated EPCs displayed a round or spindle-shaped morphology on day 5 of culture. G, On day 10, EPCs formed typical cell clusters. H, After 2 weeks of culture, EPCs showed a cobblestone-like morphology. I, EPCs cultured on Matrigel showed tube-like structures. J, The ability of EPCs to take up DiI-Ac-LDL and bind FITC-UEA-1. K, Flow cytometry analysis of the expression of EPC surface markers. Scale bar in A-D and F-J = 100 μm. ALP, alkaline phosphatase; BMSCs, bone marrow mesenchymal stem cells; EPCs, endothelial progenitor cell

(Figure 5B), the trabecular bone parameters, BMD and BV/TV exhibited higher values in this group than the other four.

An histological evaluation of bone reparation was also performed by H&E staining. As shown (Figure 5C,D), the CD and CMC/ALG groups displayed more empty lacunae than the other groups. The CMC/ALG/BMSC and CMC/ALG/EPC groups showed reduced numbers of empty lacuna (Figure 5C,D). However, the ratio of empty lacunae in the CMC/ALG/BMSC/EPC

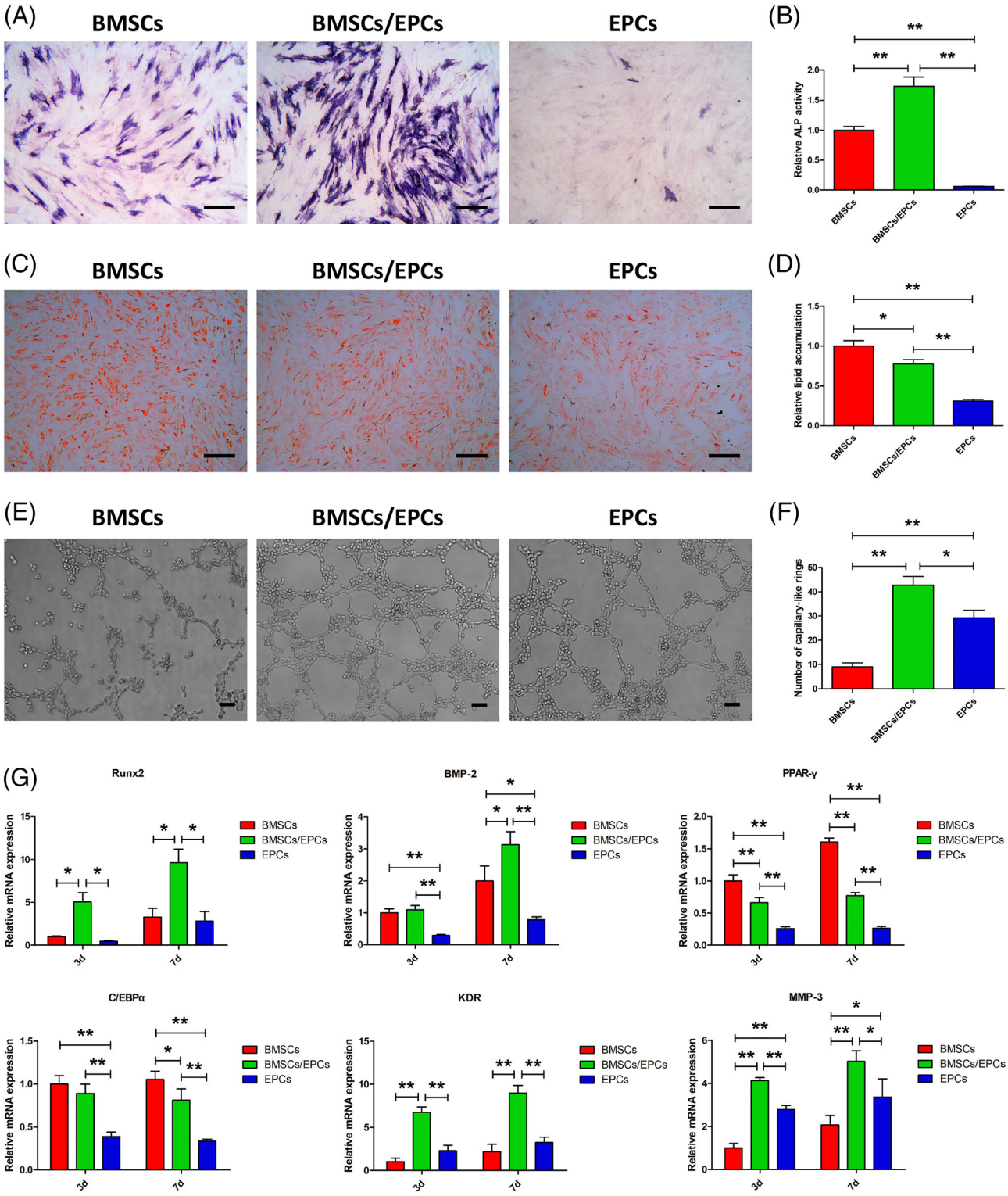

FIGURE 2 Osteogenic, adipogenic, and angiogenic differentiation abilities of BMSCs, EPCs, and cocultured cells. A, ALP staining on day 7 of osteogenic induction. B, ALP activity assay on day 7 of osteogenic induction. C, Oil red O staining on day 7 of adipogenic induction. D, Lipid accumulation assay on day 7 of adipogenic induction. E, Tube formation assay on day 7 of angiogenic differentiation. F, Quantitative analysis of number of capillary-like rings from E. G, Relative mRNA expression of osteogenesis-related genes (Runx2, BMP-2), adipogenesis-related genes (PPAR-γ, C/EBPα), and angiogenesis-related genes (KDR, MMP-3). Scale bar in A, C, and E = 100 μm. $^{*}P < .05$, $^{**}P < .01$. ALP, alkaline phosphatase

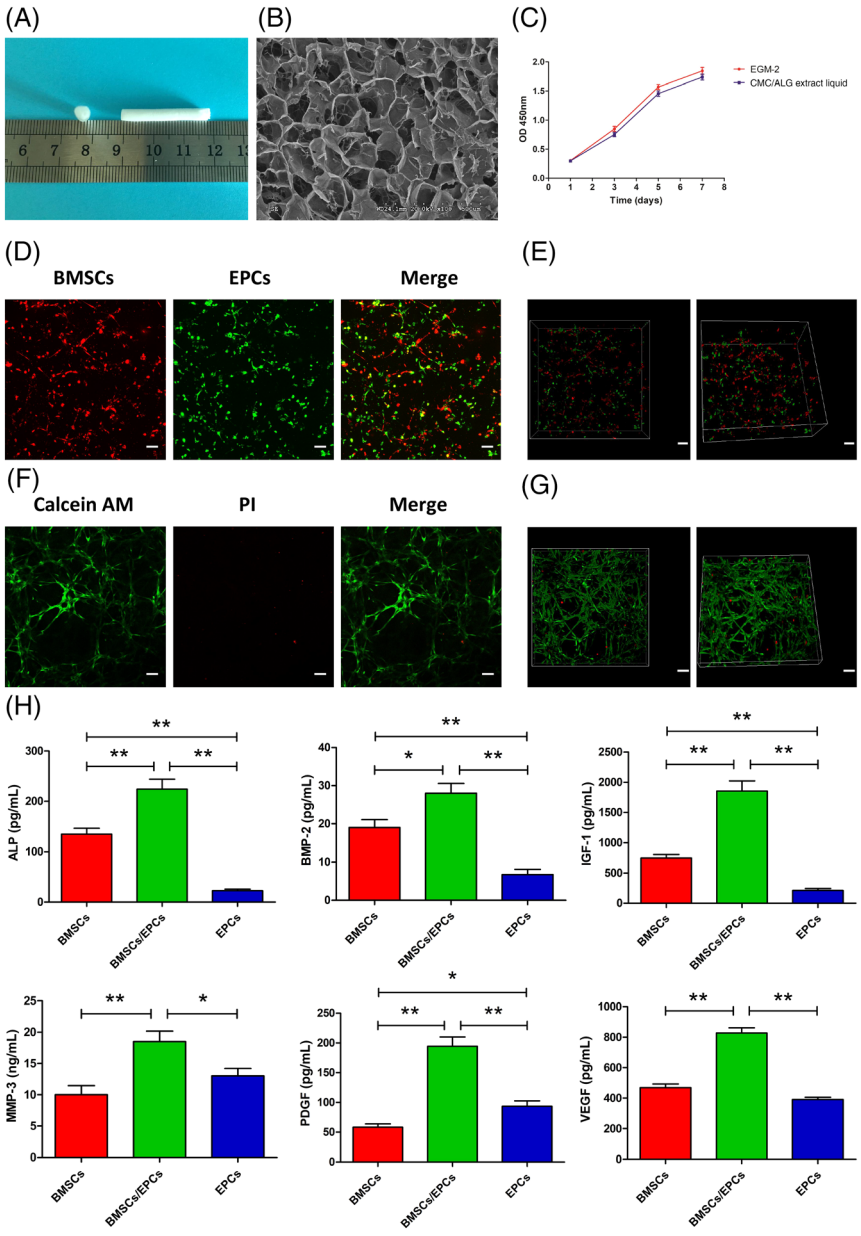

FIGURE 3 Biocompatibility of CMC/ALG scaffold and cytokine secretion of BMSCs, EPCs, and cocultured cells in 3D culture system. A, Morphology of the scaffold for in vivo transplantation. B, The SEM micrograph showed the porous structure of the scaffold. C, Effects of EGM-2 preconditioned with or without CMC/ALG scaffold on the activity of cocultured cells. D, DiI labeled BMSCs and DiO labeled EPCs adhered on the scaffold. E, 3D distribution of cocultured cells in the scaffold. F, Angiogenic differentiation and live/dead staining of cocultured cells in the CMC/ALG scaffold. G, 3D distribution of live/dead cells and tube-like structures. H, Secretion of osteogenic and angiogenic factors by BMSCs, EPCs, and cocultured cells seeded in the scaffold. Scale bar in D-G = 100 μm. $^{*}P < .05$, $^{**}P < .01$. 3D, three-dimensional; ALG, alginate; BMSCs, bone marrow mesenchymal stem cells; CMC, carboxymethyl chitosan; EPCs, endothelial progenitor cell; SEM, scanning electron microscopy

group was significantly lower than the other groups (Figure 5C,D).

3.6 | CMC/ALG/BMSC/EPC transplantation enhances osteogenic and angiogenic differentiation and reduces adipogenic differentiation

To further evaluate the reparation effects of composite implants on steroid-induced ONFH, osteogenic, adipogenic, and angiogenic differentiation capabilities in the femoral head were evaluated by immunohistochemistry. OCN staining revealed that the CD and CMC/ALG groups exhibited fewer OCN-positive cells when compared with the other groups (Figure 6A,B). The CMC/ALG/BMSC group showed more OCN-positive cells than the CMC/ALG/EPC group (Figure 6A,B). However, much more OCN-positive cells were observed in the CMC/ALG/BMSC/EPC group than any other groups (Figure 6A,B). Adiponectin staining revealed that more adiponectin-positive cells were observed in the CD and CMC/ALG groups than all other groups (Figure 6A,C). Adiponectin-positive cells in the CMC/ALG/BMSC and CMC/ALG/EPC groups were fewer than those observed in the CD and CMC/ALG groups, while the CMC/ALG/BMSC/EPC group revealed much less adiponectin-positive cells than the other groups (Figure 6A,C). CD31 staining indicated that more vessels were observed in the CMC/ALG/BMSC/EPC group when compared with the other groups (Figure 6A,D). The CMC/ALG/EPC group exhibited more vessels than the CMC/ALG/BMSC group, and both groups had more vessels than the CD and CMC/ALG groups (Figure 6A,D). These observations indicated that CMC/ALG/BMSCs/EPCs enhanced

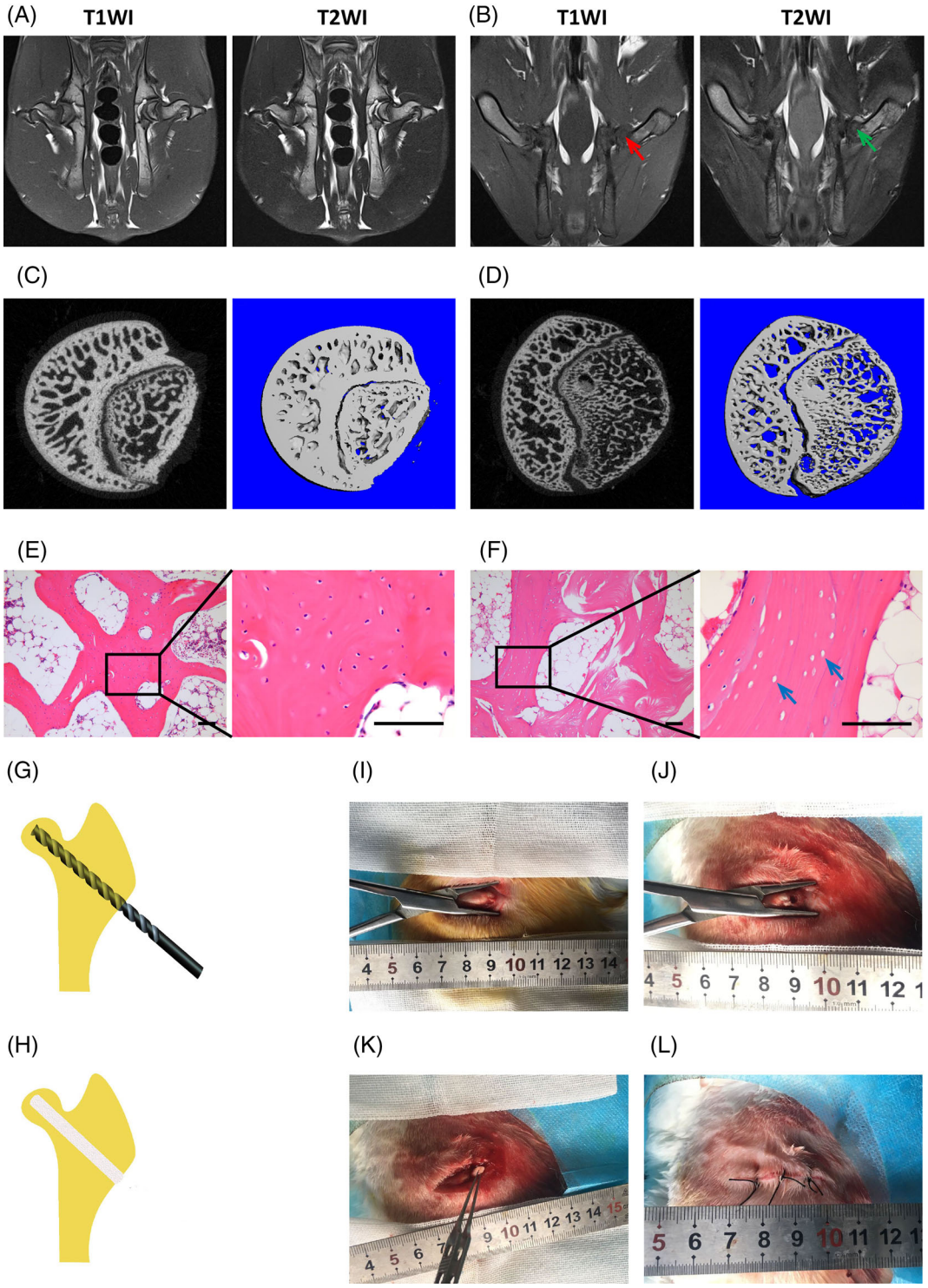

FIGURE 4 Establishment of a rabbit model of steroid-induced ONFH and the surgical procedure. A, Representative MRI photograph of the normal rabbit. B, Representative MRI photograph of the rabbit model. The red arrow indicated low signal in T1WI and the green arrow showed high signal in T2WI. C, 2D and 3D micro-CT images of the femoral head in normal group. D, 2D and 3D micro-CT images of the femoral head in model group. E, H&E staining of the normal femoral head. F, H&E staining of the necrotic femoral head. The blue arrows exhibited the empty lacuna in the necrotic region. G, illustration of core decompression. H, illustration of transplantation surgery. I, The surgical incision and greater trochanter of the femur. J, The bone tunnel with a 3 mm diameter created by core decompression. K, Transplantation process of the composite implant. L, Final suture of the incision. Scale bar in E and F = 100 μm. 2D, two-dimensional; 3D, three-dimensional; H&E, hematoxylin and eosin; MRI, magnetic resonance imaging; ONFH, osteonecrosis of the femoral head; T2WI, T2-weighted MRI images

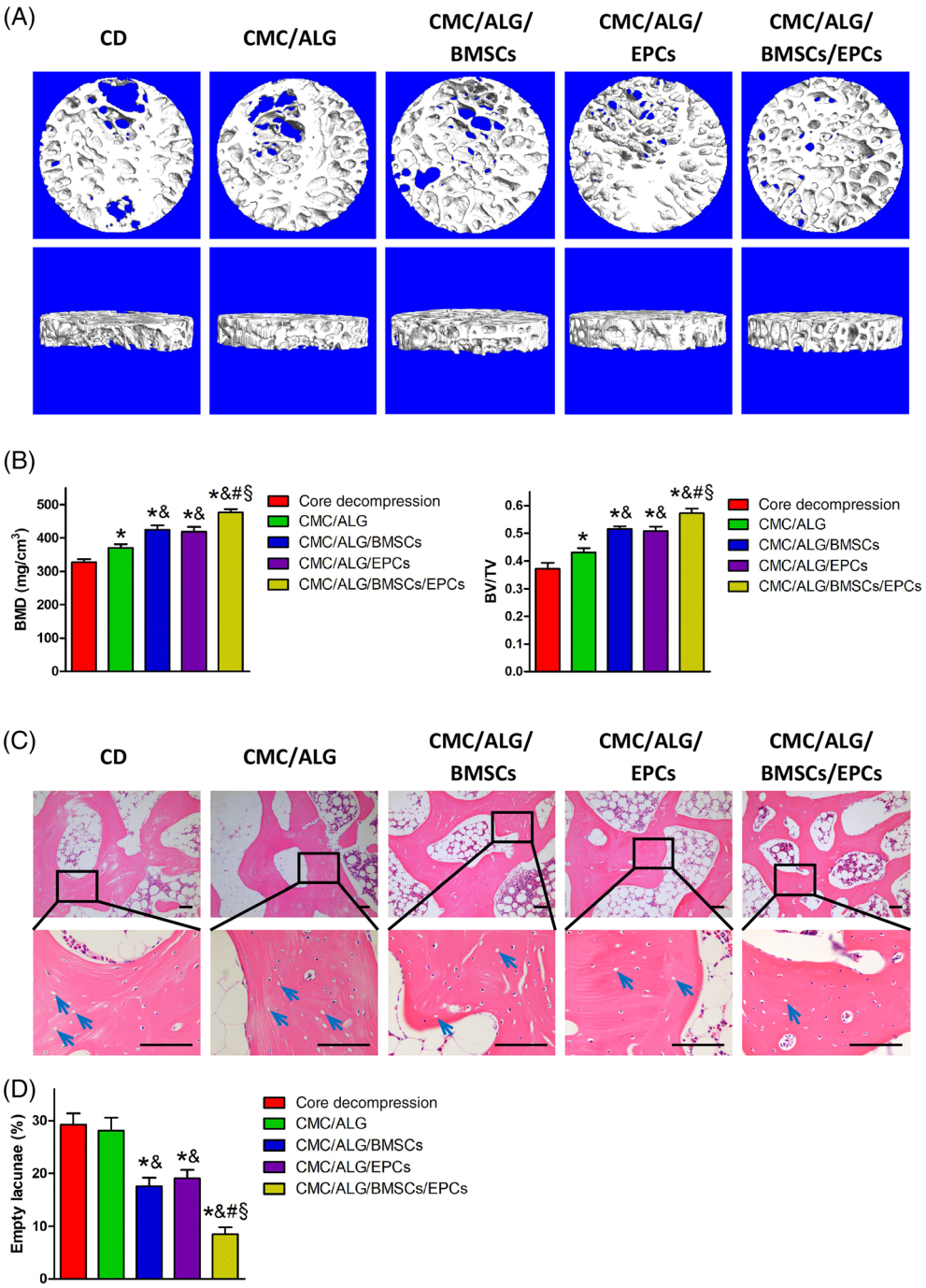

FIGURE 5 Repair of steroid-induced ONFH in each group by radiologic and histological evaluation. A, 3D micro-CT images of the subchondral region of the femoral head in each group. B, Trabecular bone parameters (BMD, BV/TV) based on reconstructed 3D images showed in Figure 5A. C, H&E staining of the empty lacuna in the necrotic region of the femoral head. The blue arrows showed the empty lacuna in the necrotic region. Scale bar = 100 μm. D, The percentage of empty lacuna in each group. Significance compared with CD group (*), CMC/ALG group (&), CMC/ALG/BMSCs group (#), and CMC/ALG/EPCs group (§). ALG, alginate; BMD, bone mineral density; BMSCs, bone marrow mesenchymal stem cells; BV/TV, bone volume/total volume; CMC, carboxymethyl chitosan; EPCs, endothelial progenitor cell; H&E, hematoxylin and eosin; ONFH, osteonecrosis of the femoral head

steroid-induced ONFH repair by promoting osteogenic and angiogenic differentiation, but reducing adipogenic differentiation.

4 | DISCUSSION

Previous studies have shown that steroid-induced ONFH results from decreased number and function of stem/progenitor cells, increased bone marrow adipocytes and increased intraosseous pressure.[35-37] Several studies have broadly investigated the treatment of steroid-induced ONFH using a combination of core decompression and tissue engineering implants.[27,38] In our study, we constructed CMC/ALG/BMSC/EPC implants, and confirmed their effects in repairing steroid-induced ONFH. To our knowledge, this is the first study exploring the efficacy of BMSCs and EPCs seeded in 3D scaffolds, for the treatment of steroid-induced ONFH.

In regenerative medicine, BMSCs are regarded as viable and feasible seeding cells for tissue engineering. Several studies have reported that BMSCs can reconstruct impaired tissues, including bone, skeletal muscle, spinal cord and liver.[39,40] EPCs have also been successfully used in cell therapy, especially for treating ischemic diseases.[41] As tissue regeneration is tightly related with the restoration of blood

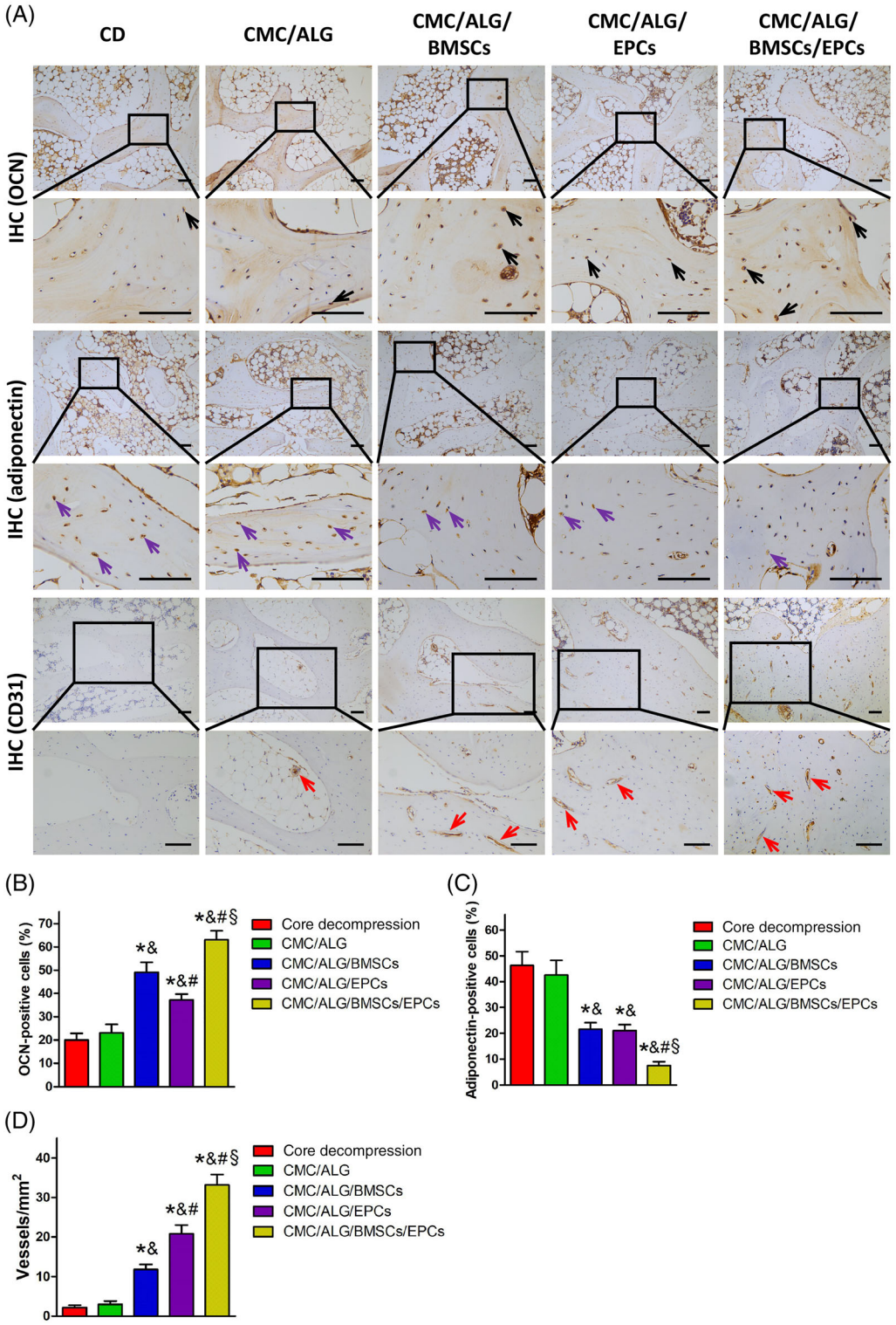

FIGURE 6 Osteogenesis, adipogenesis, and angiogenesis of the femoral head in each group by immunohistochemical analysis. A, OCN, adiponectin, and CD31 immunohistochemistry of the femoral head in each group. The black arrows showed the OCN-positive cells. The purple arrows showed the adiponectin-positive cells. The red arrows showed the vessels. Scale bar = 100 μm. B, The percentage of OCN-positive cells in each group. C, The percentage of adiponectin-positive cells in each group. D, The density of vessels in each group. Significance compared with CD group (*), CMC/ALG group (&), CMC/ALG/BMSCs group (#), and CMC/ALG/EPCs group (§). ALG, alginate; BMSCs, bone marrow mesenchymal stem cells; CD, core decompression; CMC, carboxymethyl chitosan; OCN, osteocalcin

circulation, the combined use of BMSCs and EPCs has been widely used for tissue engineering applications. In bone defect models, BMSCs and EPCs participate in bone repair via direct and indirect mechanisms. BMSCs promote bone regeneration by differentiating into osteoblasts, and EPCs facilitate the vascularization of scaffolds and implant survival by differentiating into vascular endothelial cells.[42] A mutual promotion between BMSCs and EPCs in terms of differentiation abilities, also favors the regeneration of bone and blood vessels.[43,44] Consistent with previous reports, our in vitro study concluded that BMSC/EPC coculture systems displayed enhanced osteogenic and angiogenic abilities. By establishing a steroid-induced ONFH rabbit model, we showed that cocultured cells strongly stimulated bone regeneration and neovascularization in osteonecrotic regions.

The major mechanisms that underlie cocultured pro-osteogenic and pro-angiogenic effects are believed to be mediated by paracrine actions and cell-cell contacts. In this study, we showed that BMSCs and EPCs interacted by secreting various growth factors, such as VEGF and PDGF. It was reported that BMSCs mediate EPC differentiation into endothelial cells by secreting VEGF.[45] It has also been demonstrated that EPCs promote osteogenesis in BMSCs by acting the role of growth factors and adding VEGF into BMSCs/EPCs/scaffold complexes to repair bone defects was unnecessary.[46] Similarly, Liang et al showed that BMSC and EPC coculture enhanced PDGF secretion and their angiogenesis.[21]

Both BMSCs and EPCs originate from the bone marrow niche, where they interact via direct contact. A previous study demonstrated that endothelial cells or EPCs facilitate BMSC differentiation into endothelial-like phenotypes via a contact-based method.[47] Aguirre et al reported that both BMSCs and EPCs contributed to the formation of tube-like structures in coculture systems.[48] It was also demonstrated that heterotypic cell contacts between T17b EPCs and BMSCs contributed to the enhanced production of MMP-3, an important angiogenic protease.[22] Additionally, a 3D porous scaffold containing BMSCs and EPCs was shown to promote bone formation by facilitating cell-cell contacts and the formation of junctional proteins.[49]

Apart from impaired osteogenesis and angiogenesis, lipid metabolism disorder is another crucial factor contributing to steroid-induced ONFH. Adipocyte hypertrophy and fat embolisms can directly cause vascular occlusion of the femoral head.[50] Previous studies have reported that excessive lipid accumulation in the femoral head disrupted the balance between osteogenic and adipogenic differentiation of BMSCs.[35,51] Transcription factors and transforming growth factors also play central roles in deciding the fate of MSCs; for example, Runx2 and BMP-2 are major transcription factors that regulate MSC osteogenic differentiation. Cells with impaired Runx2 do not acquire osteoblastic phenotypes, but instead exhibit adipocyte phenotypes.[52] The high expression of BMP-2 also promotes osteogenic differentiation and inhibits adipogenic differentiation.[53] PPARγ and C/EBPα are key adipogenic differentiation transcription factors for MSCs. It was reported that PPARγ expression accelerated adipogenic differentiation and suppressed the osteogenic differentiation of BMSCs.[54] Repression of C/EBPα expression was shown to decrease adipogenesis and lipid accumulation.[55] In our study, we showed that BMSCs cocultured with EPCs were inclined to differentiate into osteogenic cells, rather than adipose cells. Our index analysis of osteogenic and adipogenic differentiation in cocultured cells showed elevated Runx2 and BMP-2 expression, while PPARγ and C/EBPα expression was decreased. By transplanting BMSCs and EPCs into the femoral head, we observed that the percentage of OCN-positive cells was increased, while adiponectin-positive cells exhibited decreased ratios. Thus, we showed that BMSC and EPC cotransplantation was beneficial for balanced osteogenesis and adipogenesis in the femoral head.

The 3D scaffold is an important component of tissue engineering, especially for treating ONFH. Scaffolds induce bone ingrowth by facilitating bridging structures between the bone tunnel and nearby bone tissue, reducing the risk of subchondral fracture and femoral head collapse. More importantly, the scaffold promotes osteogenesis by favoring the loading and interaction of seeded cells in the 3D space.[49] To fully reveal the biological effects of BMSCs and EPCs in the femoral head, we fabricated CMC/ALG scaffolds. No toxic organic solvents were used in the preparation of these scaffolds, thus ensuring a safe and noncytotoxic area for seeded cells. Apart from cytotoxicity, scaffold porosity was another important consideration for cell adhesion and proliferation.[56] Our scaffolds promoted cell adhesion, and we believe this characteristic contributes to its noncytotoxicity and porous nature. Our in vivo studies showed that CMC/ALG scaffolds, seeded with either BMSCs or EPCs enhanced ONFH repair, however, greater bone and blood vessel densities were observed in the CMC/ALG/BMSC/EPC group. Although CMC/ALG scaffolds alone promoted some bone repair, the reparation effects were far from satisfactory due to a shortage of osteogenic and angiogenic cells in the necrotic femoral head. Thus, our strategy may improve the clinical outcomes for early stage steroid-induced ONFH.

It was reported that implanted cells may promote tissue regeneration via engraftment, differentiation and paracrine actions.[57] While these cells can directly engraft and differentiate into target tissues, they can also secrete growth factors and cytokines which facilitate tissue repair by stimulating endogenous cell activity.[58] However, in our study, we believe that the bone reparation mainly benefits from engraftment and differentiation of implanted cells, instead of paracrine-induced indirect action. Several studies have showed that the number and function of stem/progenitor cells in patients with steroid-induced ONFH are obviously decreased, which is why most patients treated with autologous stem cells eventually progress to femoral head collapse.[35-37] Thus, endogenous stem/progenitor cells have limited effects on the repair of steroid-induced ONFH.

Our study had some limitations. First, we established cell coculture and cotransplantation systems in a 1:1 ratio. However, the optimal ratio for repairing steroid-induced ONFH is currently unknown, and therefore requires further study. Previous studies have reported that different MSC and EPC ratios generated different biological effects; He et al reported that the best coculture ratio for BMSCs and EPCs in terms of osteogenic differentiation was 1:1.[24] Similarly, Liang et al showed that proliferation rates were highest

when EPCs and BMSCs were cultured in a 1:1 ratio.[59] Fu et al demonstrated that a 3:1 ratio of peripheral blood-derived MSCs to EPCs exhibited the highest osteogenic and angiogenic marker expression.[60] Thus, tissue source of MSCs and EPCs are likely to be key factors in defining optimal ratios. Second, the mechanical strength of CMC/ALG scaffolds was not as good as autologous bone and tantalum rods. Therefore, improvements in the mechanical properties of scaffolds are warranted, and could contribute to clinical applications. Third, according to previous reports, oxygen levels in the necrotic area of the femoral head are quite low when compared with the normal femoral head.[61,62] Thus, for future studies, researchers must ascertain the in vitro differentiation capabilities of cocultured cells under hypoxic conditions.

5 | CONCLUSION

Our study suggests that CMC/ALG/BMSC/EPC composite implants promote the repair of steroid-induced ONFH by enhancing osteogenesis and angiogenesis, and reducing adipogenesis. Thus, in combination with core decompression, the cotransplantation of BMSCs and EPCs on 3D scaffolds may be a potential therapeutic strategy for steroid-induced ONFH.

ACKNOWLEDGMENT

This work was supported by grants from National Natural Science Foundation of China (grant numbers 81672140 and 81974329) and Natural Science Foundation of Guangdong Province (grant numbers 2017A030313111 and 2017A030312009).

CONFLICT OF INTEREST

The authors declared no potential conflicts of interest.

AUTHOR CONTRIBUTIONS

H.X., C.W.: conception and design, data analysis and interpretation, manuscript writing, final approval of manuscript; C.L.: conception and design, data analysis and interpretation, final approval of manuscript; Z.P., J.L., Y.J., Y.W.: data analysis and interpretation, final approval of manuscript; J.G.: supervision of research work, final approval of manuscript; L.Z.: financial support, supervision of research work, final approval of manuscript.

DATA AVAILABILITY STATEMENT

The data that support the findings of this study are available from the corresponding author upon reasonable request.

ORCID

Lixin Zhu https://orcid.org/0000-0003-3055-3063

REFERENCES

1. Nishii T, Sugano N, Ohzono K, Sakai T, Haraguchi K, Yoshikawa H. Progression and cessation of collapse in osteonecrosis of the femoral head. *Clin Orthop Relat Res*. 2002;400:149-157.
2. Morita D, Hasegawa Y, Okura T, et al. Long-term outcomes of transtrochanteric rotational osteotomy for non-traumatic osteonecrosis of the femoral head. *Bone Joint J*. 2017;99-B:175-183.
3. Mont MA, Hungerford DS. Non-traumatic avascular necrosis of the femoral head. *J Bone Joint Surg Am*. 1995;77:459-474.
4. Sakaguchi M, Tanaka T, Fukushima W. Impact of oral corticosteroid use for idiopathic osteonecrosis of the femoral head: a nationwide multicenter case-control study in Japan. *J Orthop Sci*. 2010;15:185-191.
5. Wang A, Ren M, Wang J. The pathogenesis of steroid-induced osteonecrosis of the femoral head: a systematic review of the literature. *Gene*. 2018;671:103-109.
6. Ohzono K, Takaoka K, Saito S, et al. Intraosseous arterial architecture in nontraumatic avascular necrosis of the femoral head. Microangiographic and histologic study. *Clin Orthop Relat Res*. 1992;277:79-88.
7. Koo KH, Kim R, Ko GH, et al. Preventing collapse in early osteonecrosis of the femoral head. A randomised clinical trial of core decompression. *J Bone Joint Surg Br*. 1995;77:870-874.
8. Xie H, Wang B, Tian S, Liu B, Qin K, Zhao D. Retrospective long-term follow-up survival analysis of the management of osteonecrosis of the femoral head with pedicled vascularized iliac bone graft transfer. *J Arthroplasty*. 2019;34:1585-1592.
9. Johnson AJ, Mont MA, Tsao AK, Jones LC. Treatment of femoral head osteonecrosis in the United States: 16-year analysis of the nationwide inpatient sample. *Clin Orthop Relat Res*. 2014;472:617-623.
10. Bergh C, Fenstad AM, Furnes O, et al. Increased risk of revision in patients with non-traumatic femoral head necrosis. *Acta Orthop*. 2014;85:11-17.
11. Dale H, Fenstad AM, Hallan G, et al. Increasing risk of prosthetic joint infection after total hip arthroplasty. *Acta Orthop*. 2012;83:449-458.
12. Kang JS, Suh YJ, Moon KH, et al. Clinical efficiency of bone marrow mesenchymal stem cell implantation for osteonecrosis of the femoral head: a matched pair control study with simple core decompression. *Stem Cell Res Ther*. 2018;9:274.
13. Wen Q, Ma L, Chen YP, Yang L, Luo W, Wang XN. Treatment of avascular necrosis of the femoral head by hepatocyte growth factor-transgenic bone marrow stromal stem cells. *Gene Ther*. 2008;15:1523-1535.
14. Wen Q, Jin D, Zhou CY, Zhou MQ, Luo W, Ma L. HGF-transgenic MSCs can improve the effects of tissue self-repair in a rabbit model of traumatic osteonecrosis of the femoral head. *PLoS One*. 2012;7:e37503.
15. Kong Y, Zhao Y, Li D, Shen H, Yan M. Dual delivery of encapsulated BM-MSCs and BMP-2 improves osteogenic differentiation and new bone formation. *J Biomed Mater Res A*. 2019;107:2282-2295.
16. Deng M, Chang Z, Hou T, et al. Sustained release of bioactive protein from a lyophilized tissue-engineered construct promotes the osteogenic potential of mesenchymal stem cells. *J Orthop Res*. 2016;34:386-394.
17. Shapiro G, Lieber R, Gazit D, Pelled G. Recent advances and future of gene therapy for bone regeneration. *Curr Osteoporos Rep*. 2018;16:504-511.
18. Amsden B. Novel biodegradable polymers for local growth factor delivery. *Eur J Pharm Biopharm*. 2015;97:318-328.
19. Sun Y, Feng Y, Zhang C, et al. Beneficial effect of autologous transplantation of endothelial progenitor cells on steroid-induced femoral head osteonecrosis in rabbits. *Cell Transplant*. 2011;20:233-243.
20. Li Q, Wang Z. Influence of mesenchymal stem cells with endothelial progenitor cells in co-culture on osteogenesis and angiogenesis: an in vitro study. *Arch Med Res*. 2013;44:504-513.
21. Liang T, Zhu L, Gao W, et al. Coculture of endothelial progenitor cells and mesenchymal stem cells enhanced their proliferation and angiogenesis through PDGF and notch signaling. *FEBS Open Bio*. 2017;7:1722-1736.

22. Steiner D, Köhn K, Beier JP, Stürzl M, Horch RE, Arkudas A. Cocultivation of mesenchymal stem cells and endothelial progenitor cells reveals antiapoptotic and proangiogenic effects. *Cells Tissues Organs*. 2017;204:218-227.
23. Zigdon-Giladi H, Bick T, Lewinson D, Machtei EE. Co-transplantation of endothelial progenitor cells and mesenchymal stem cells promote neovascularization and bone regeneration. *Clin Implant Dent Relat Res*. 2015;17:353-359.
24. He X, Dziak R, Yuan X, et al. BMP2 genetically engineered MSCs and EPCs promote vascularized bone regeneration in rat critical-sized calvarial bone defects. *PLoS One*. 2013;8:e60473.
25. Daltro GC, Fortuna V, de Souza ES, et al. Efficacy of autologous stem cell-based therapy for osteonecrosis of the femoral head in sickle cell disease: a five-year follow-up study. *Stem Cell Res Ther*. 2015;6:110.
26. Yamasaki T, Yasunaga Y, Ishikawa M, et al. Bone-marrow-derived mononuclear cells with a porous hydroxyapatite scaffold for the treatment of osteonecrosis of the femoral head: a preliminary study. *J Bone Joint Surg Br*. 2010;92:337-341.
27. Maruyama M, Nabeshima A, Pan CC, et al. The effects of a functionally-graded scaffold and bone marrow-derived mononuclear cells on steroid-induced femoral head osteonecrosis. *Biomaterials*. 2018;187:39-46.
28. Vahidy FS, Rahbar MH, Zhu H, et al. Systematic review and meta-analysis of bone marrow-derived mononuclear cells in animal models of ischemic stroke. *Stroke*. 2016;47:1632-1639.
29. Hu L, Yin C, Zhao F, Ali A, Ma J, Qian A. Mesenchymal stem cells: cell fate decision to osteoblast or adipocyte and application in osteoporosis treatment. *Int J Mol Sci*. 2018;19:360.
30. Upadhyaya L, Singh J, Agarwal V, Tewari RP. Biomedical applications of carboxymethyl chitosans. *Carbohydr Polym*. 2013;91:452-466.
31. Jain D, Bar-Shalom D. Alginate drug delivery systems: application in context of pharmaceutical and biomedical research. *Drug Dev Ind Pharm*. 2014;40:1576-1584.
32. Lu Y, Li L, Zhu Y, et al. Multifunctional copper-containing carboxymethyl chitosan/alginate scaffolds for eradicating clinical bacterial infection and promoting bone formation. *ACS Appl Mater Interfaces*. 2018;10:127-138.
33. Pang H, Wu XH, Fu SL, et al. Prevascularisation with endothelial progenitor cells improved restoration of the architectural and functional properties of newly formed bone for bone reconstruction. *Int Orthop*. 2013;37:753-759.
34. Zhu H, Cai X, Lin T, Shi Z, Yan S. Low-intensity pulsed ultrasound enhances bone repair in a rabbit model of steroid-associated osteonecrosis. *Clin Orthop Relat Res*. 2015;473:1830-1839.
35. Houdek MT, Wyles CC, Packard BD, Terzic A, Behfar A, Sierra RJ. Decreased osteogenic activity of mesenchymal stem cells in patients with corticosteroid-induced osteonecrosis of the femoral head. *J Arthroplasty*. 2016;31:893-898.
36. Feng Y, Yang SH, Xiao BJ, et al. Decreased in the number and function of circulation endothelial progenitor cells in patients with avascular necrosis of the femoral head. *Bone*. 2010;46:32-40.
37. Wang T, Teng S, Zhang Y, Wang F, Ding H, Guo L. Role of mesenchymal stem cells on differentiation in steroid-induced avascular necrosis of the femoral head. *Exp Ther Med*. 2017;13:669-675.
38. Zhang HX, Zhang XP, Xiao GY, et al. In vitro and in vivo evaluation of calcium phosphate composite scaffolds containing BMP-VEGF loaded PLGA microspheres for the treatment of avascular necrosis of the femoral head. *Korean J Couns Psychother*. 2016;60:298-307.
39. Han Y, Li X, Zhang Y, Han Y, Chang F, Ding J. Mesenchymal stem cells for regenerative medicine. *Cell*. 2019;8:886.
40. Kariminekoo S, Movassaghpour A, Rahimzadeh A, Talebi M, Shamsasenjan K, Akbarzadeh A. Implications of mesenchymal stem cells in regenerative medicine. *Artif Cells Nanomed Biotechnol*. 2016;44:749-757.
41. Alev C, Ii M, Asahara T. Endothelial progenitor cells: a novel tool for the therapy of ischemic diseases. *Antioxid Redox Signal*. 2011;15:949-965.
42. Seebach C, Henrich D, Wilhelm K, Barker JH, Marzi I. Endothelial progenitor cells improve directly and indirectly early vascularization of mesenchymal stem cell-driven bone regeneration in a critical bone defect in rats. *Cell Transplant*. 2012;21:1667-1677.
43. Seebach C, Henrich D, Kähling C, et al. Endothelial progenitor cells and mesenchymal stem cells seeded onto beta-TCP granules enhance early vascularization and bone healing in a critical-sized bone defect in rats. *Tissue Eng Part A*. 2010;16:1961-1970.
44. Li Z, Yang A, Yin X, et al. Mesenchymal stem cells promote endothelial progenitor cell migration, vascularization, and bone repair in tissue-engineered constructs via activating CXCR2-Src-PKL/Vav2-Rac1. *FASEB J*. 2018;32:2197-2211.
45. Ge Q, Zhang H, Hou J, et al. VEGF secreted by mesenchymal stem cells mediates the differentiation of endothelial progenitor cells into endothelial cells via paracrine mechanisms. *Mol Med Rep*. 2018;17:1667-1675.
46. Khojasteh A, Fahimipour F, Jafarian M, et al. Bone engineering in dog mandible: coculturing mesenchymal stem cells with endothelial progenitor cells in a composite scaffold containing vascular endothelial growth factor. *J Biomed Mater Res B Appl Biomater*. 2017;105:1767-1777.
47. Joddar B, Kumar SA, Kumar A. A contact-based method for differentiation of human mesenchymal stem cells into an endothelial cell-phenotype. *Cell Biochem Biophys*. 2018;76:187-195.
48. Aguirre A, Planell JA, Engel E. Dynamics of bone marrow-derived endothelial progenitor cell/mesenchymal stem cell interaction in co-culture and its implications in angiogenesis. *Biochem Biophys Res Commun*. 2010;400:284-291.
49. Guerrero J, Catros S, Derkaoui SM, et al. Cell interactions between human progenitor-derived endothelial cells and human mesenchymal stem cells in a three-dimensional macroporous polysaccharide-based scaffold promote osteogenesis. *Acta Biomater*. 2013;9:8200-8213.
50. Fukui K, Kominami R, Shinohara H, Matsumoto T. Glucocorticoid induces micro-fat embolism in the rabbit: a scanning electron microscopic study. *J Orthop Res*. 2006;24:675-683.
51. Sheng HH, Zhang GG, Cheung WH, et al. Elevated adipogenesis of marrow mesenchymal stem cells during early steroid-associated osteonecrosis development. *J Orthop Surg Res*. 2007;2:15.
52. Kobayashi H, Gao Y, Ueta C, Yamaguchi A, Komori T. Multilineage differentiation of Cbfa1-deficient calvarial cells in vitro. *Biochem Biophys Res Commun*. 2000;273:630-636.
53. Wang EA, Israel DI, Kelly S, Luxenberg DP. Bone morphogenetic protein-2 causes commitment and differentiation in C3H10T1/2 and 3T3 cells. *Growth Factors*. 1993;9:57-71.
54. Zhang LY, Xue HG, Chen JY, et al. Genistein induces adipogenic differentiation in human bone marrow mesenchymal stem cells and suppresses their osteogenic potential by upregulating PPARγ. *Exp Ther Med*. 2016;11:1853-1858.
55. Li D, Zhu H, Liang C, et al. CKIP-1 suppresses the adipogenesis of mesenchymal stem cells by enhancing HDAC1-associated repression of C/EBPα. *J Mol Cell Biol*. 2014;6:368-379.
56. Low SP, Williams KA, Canham LT, et al. Evaluation of mammalian cell adhesion on surface-modified porous silicon. *Biomaterials*. 2006;27:4538-4546.
57. García-Sánchez D, Fernández D, Rodríguez-Rey JC, et al. Enhancing survival, engraftment, and osteogenic potential of mesenchymal stem cells. *World J Stem Cells*. 2019;11:748-763.
58. Horwitz EM, Dominici M. How do mesenchymal stromal cells exert their therapeutic benefit? *Cytotherapy*. 2008;10:771-774.
59. Liang Y, Wen L, Shang F, Wu J, Sui K, Ding Y. Endothelial progenitors enhanced the osteogenic capacities of mesenchymal stem cells

in vitro and in a rat alveolar bone defect model. *Arch Oral Biol*. 2016; 68:123-130.
60. Fu WL, Xiang Z, Huang FG, et al. Coculture of peripheral blood-derived mesenchymal stem cells and endothelial progenitor cells on strontium-doped calcium polyphosphate scaffolds to generate vascularized engineered bone. *Tissue Eng Part A*. 2015;21:948-959.
61. Kiaer T, Pedersen NW, Kristensen KD, et al. Intra-osseous pressure and oxygen tension in avascular necrosis and osteoarthritis of the hip. *J Bone Joint Surg Br*. 1990;72:1023-1030.
62. Watanabe Y, Terashima Y, Takenaka N, Kobayashi M, Matsushita T. Prediction of avascular necrosis of the femoral head by measuring intramedullary oxygen tension after femoral neck fracture. *J Orthop Trauma*. 2007;21:456-461.

SUPPORTING INFORMATION

Additional supporting information may be found online in the Supporting Information section at the end of this article.

How to cite this article: Xu H, Wang C, Liu C, et al. Cotransplantation of mesenchymal stem cells and endothelial progenitor cells for treating steroid-induced osteonecrosis of the femoral head. *STEM CELLS Transl Med*. 2021;10:781–796. https://doi.org/10.1002/sctm.20-0346